Supplementary material for "Simultaneous reduction of number of spots and energy layers in intensity modulated proton therapy for rapid spot scanning delivery"

Anqi Fu[1], Vicki T. Taasti[2], Masoud Zarepisheh[1]
[1] Department of Medical Physics, Memorial Sloan Kettering Cancer Center, New York, NY 10065, USA
[2] Danish Center for Particle Therapy, Aarhus University Hospital, Aarhus 8200, Denmark

Anqi Fu. 321 East 61st Street, New York, NY 10065, USA. email: fua@mskcc.org

SI. Derivation of problem 3

Problem 2 in the main text is a nonconvex optimization problem because the equality constraints $\overline{d} = (Ax - p)_+$ and $\underline{d} = (Ax - p)_-$ are nonlinear. We will show that it is equivalent to the convex optimization problem 3, which replaces the nonlinear equality constraints with the linear equality constraint $Ax - \overline{d} + \underline{d} = p$. Since the objective functions are identical, it is sufficient to prove that any solution of problem 2 is a feasible point for problem 3 and vice versa.

Let $v^\star := (x^\star, \overline{d}^\star, \underline{d}^\star)$ be a solution of problem 2. Then,

$$\begin{aligned} Ax^\star - \overline{d}^\star + \underline{d}^\star - p &= (Ax^\star - p) - (Ax^\star - p)_+ + (Ax^\star - p)_- \\ &= (Ax^\star - p) - (\max(Ax^\star - p, 0) + \min(Ax^\star - p, 0)) = 0, \end{aligned}$$

because any real function can be written as the sum of its nonnegative and nonpositive parts. Thus, $v^\star$ is feasible for problem 3, and since the two problems have the same objective function, $v^\star$ is a solution of problem 3.

Now let us show the converse. First, we will relax the equality constraints in problem 2 to get

$$\begin{array}{ll} \text{minimize} & f(\overline{d}, \underline{d}) \\ \text{subject to} & \overline{d} \geq (Ax - p)_+, \quad \underline{d} \geq (Ax - p)_-, \quad Bx \leq c \\ & x \geq 0, \quad \overline{d} \geq 0, \quad \underline{d} \geq 0. \end{array} \tag{1}$$

This relaxed problem is equivalent to problem 2 because the relaxed constraints, $\overline{d} \geq (Ax-p)_+$ and $\underline{d} \geq (Ax-p)_-$, are tight at the optimum, since the objective function 1 is monotonically increasing over the nonnegative reals. Any feasible point $(\hat{x}, \hat{\overline{d}}, \hat{\underline{d}})$ of problem 1 that does not satisfy $\hat{\overline{d}} = (A\hat{x}-p)_+$ and $\hat{\underline{d}} = (A\hat{x}-p)_-$ cannot be optimal, as we can perturb it to obtain another feasible point with a strictly lower objective value.

For example, suppose $\hat{\underline{d}}_i > \min(A\hat{x}-p, 0)_i$ for a voxel $i \in \{1, \ldots, m\}$, then we can decrease $\hat{\underline{d}}_i$ by some small quantity $\delta > 0$ to get $\tilde{\underline{d}} := \hat{\underline{d}} - \delta e_i \geq 0$ that still satisfies the inequality constraint. (Here $e_i \in \{0,1\}^n$ is the indicator vector of index i, which equals 1 at i and 0 elsewhere). The new point $(\hat{x}, \hat{\overline{d}}, \tilde{\underline{d}})$ is feasible for problem 1, but attains a lower objective $f(\hat{\overline{d}}, \tilde{\underline{d}}) < f(\hat{\overline{d}}, \hat{\underline{d}})$ because the quadratic term $\underline{w}_i \tilde{\underline{d}}_i^2 < \underline{w}_i \hat{\underline{d}}_i^2$ by our choice of $\delta > 0$, assuming $\underline{w}_i \neq 0$. If $\underline{w}_i = 0$, the underdose to voxel i has no impact on the objective and can be removed entirely from the optimization problem.

It suffices then to show that any solution $v^\star = (x^\star, \overline{d}^\star, \underline{d}^\star)$ of problem 3 is a solution of problem 1. This is true because $Ax^\star - \overline{d}^\star + \underline{d}^\star = p$ and $\overline{d}^\star \geq 0, \underline{d}^\star \geq 0$ imply

$$\begin{aligned}
\overline{d}^\star &= Ax^\star - p + \underline{d}^\star \geq Ax^\star - p, \\
\underline{d}^\star &= -(Ax^\star - p) + \overline{d}^\star \geq -(Ax^\star - p).
\end{aligned}$$

Thus, we can conclude that

$$\begin{aligned}
\overline{d}^\star &\geq \max(Ax^\star - p, 0) = (Ax^\star - p)_+, \\
\underline{d}^\star &\geq \max(-(Ax^\star - p), 0) = -\min(Ax^\star - p, 0) = (Ax^\star - p, 0)_-.
\end{aligned}$$

SII. Delivery efficiency and clinical metrics

In this section, we present further results on the delivery time and other clinical metrics. Figure S1 is an extension of Figure 8 in the main text, depicting the relative percentage change in total delivery time, number of nonzero spots/energy layers, and several dosimetric quantities at 10% cost to plan quality for patients 1, 3, and 4. Table S1 provides the absolute values for the metrics plotted in the two figures. Together, they show that reweighted l_1 regularization outperforms l_1 and group l_2 regularization in all patients.

Table S1: Values of various metrics under the unregularized plan and the l_1, group l_2, and reweighted l_1 regularized plans. For each patient and regularizer, λ was chosen such that the regularized plan resulted in a 10% cost to plan quality relative to the unregularized plan (e.g., as shown by the dotted line in Figure 5).

Patient	Metric	Unregularized	l_1	Group l_2	Reweighted l_1
1	Num. Nonzero Spots	1796	1102	4264	1061
	Num. Nonzero Layers	55	53	48	35
	Delivery Time (s)	155.41	144.49	166.16	108.26
	PTV: D2% (Gy)	71.90	73.10	73.18	72.70
	PTV: D98% (Gy)	68.17	68.46	68.29	68.34
	PTV: CI	1.40	1.37	1.38	1.40
	Mandible: Dmax (Gy)	67.49	68.50	67.62	68.77
	Parotids: Dmean (Gy)	11.50	8.96	11.53	7.95
2	Num. Nonzero Spots	2295	1182	5719	976
	Num. Nonzero Layers	67	61	52	33
	Delivery Time (s)	184.28	161.21	188.67	103.43
	PTV: D2% (Gy)	70.37	73.49	73.61	73.30
	PTV: D98% (Gy)	68.21	67.62	67.73	67.93
	PTV: CI	1.49	1.44	1.45	1.48
	Mandible: Dmax (Gy)	64.86	63.84	67.36	66.13
	Parotids: Dmean (Gy)	2.04	1.29	3.63	1.49
3	Num. Nonzero Spots	1751	1247	3738	1172
	Num. Nonzero Layers	58	55	50	41
	Delivery Time (s)	160.93	149.92	164.88	121.31
	PTV: D2% (Gy)	70.54	72.44	71.95	72.12
	PTV: D98% (Gy)	67.70	66.97	67.06	67.14
	PTV: CI	1.84	1.78	1.78	1.83
	Mandible: Dmax (Gy)	67.06	67.53	65.91	67.11
	Parotids: Dmean (Gy)	13.41	13.54	13.37	13.51
4	Num. Nonzero Spots	259	195	480	169
	Num. Nonzero Layers	37	35	36	27
	Delivery Time (s)	104.22	99.60	104.44	83.42
	PTV: D2% (Gy)	71.27	72.47	71.77	71.88
	PTV: D98% (Gy)	68.28	67.71	67.95	67.88
	PTV: CI	1.59	1.48	1.54	1.56
	Mandible: Dmax (Gy)	64.03	62.29	63.32	64.55
	Parotids: Dmean (Gy)	7.01	5.83	6.79	6.14

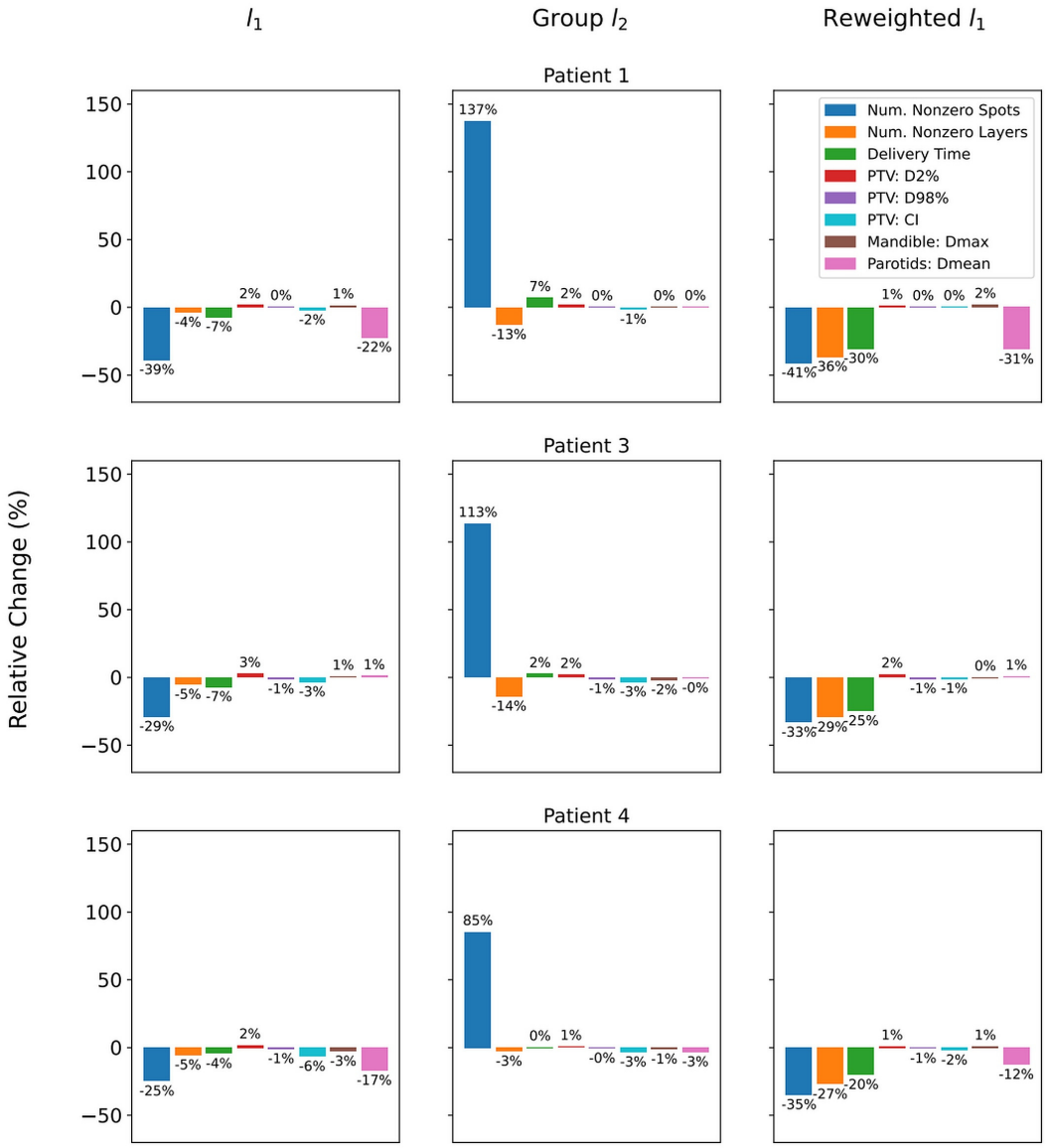

Figure S1: Relative change in delivery time and other plan metrics with respect to the unregularized model for l_1, group l_2, and reweighted l_1 regularization. For each regularizer, λ was chosen such that the regularized model resulted in about 10% cost to plan quality. Here the conformity index (CI) is defined as the total number of voxels that received at least 95% of the prescribed dose, divided by the number of voxels in the PTV[60].

SIII. Robustness analysis

To analyze the robustness of the proton plans, we generated 13 uncertainty scenarios (including the nominal scenario) by rescaling the stopping power ratio (SPR) image ±3.5% to simulate range over/undershoot errors[74,75] and shifting the isocenter ±3 mm in the x, y, and z directions to simulate setup errors. For each scenario $r \in \{1, \ldots, 13\}$, we computed the dose influence matrix $A^r \in \mathbf{R}_+^{m \times n}$. We solved the unregularized treatment planning problem 3 using only the dose influence matrix of the nominal scenario to get the optimal nominal spot vector $x^\star_{unreg}$ and calculated the dose in each scenario to be $d^r_{unreg} = A^r x^\star_{unreg}$. We repeated this process, again using only the nominal dose influence matrix in the optimization, with the reweighted l_1 regularization method to obtain doses $d^r_{rewl_1} = A^r x_{rewl_1}$. (As before, λ was chosen such that the reweighted l_1 plan results in a 10% cost to plan quality relative to the unregularized plan). In the end, for each patient, we had two sets of dose vectors representing the potential scenario outcomes if we were to treat using the unregularized plan and the reweighted l_1 regularized plan: $(d^1_{unreg}, \ldots, d^{13}_{unreg})$ and $(d^1_{rewl_1}, \ldots, d^{13}_{rewl_1})$.

Figures S2–S5 depict the DVH bands resulting from these sets of doses for each patient. Every band delineates the range of DVH curves for a particular structure, taken across all uncertainty scenarios. The corresponding solid line is the DVH curve in the nominal scenario. Generally, the DVH bands of the reweighted l_1 regularized plan are similar to those of the unregularized plan. For patients 1 and 4, the reweighted l_1 plan results in a slightly narrower PTV band (smaller range of uncertainty), while the opposite is true for patients 2 and 3. In the case of OARs, the most noticeable difference is the reweighted l_1 plan exhibits thinner bands for the mandible in patient 1, but wider bands for the left parotid in patient 3. All other structures have comparable DVH bands between the unregularized and the reweighted l_1 regularized plans. We also provide the median and range of several clinical metrics in Table S2. These values support our conclusion that the reweighted l_1 method produces a treatment plan with similar robustness to the plan generated by the unregularized model, and its resulting dose satisfies clinical constraints in the majority of our uncertainty scenarios.

Table S2: The median and range (maximum − minimum) of various metrics calculated across 13 uncertainty scenarios, using the unregularized plan and the reweighted l_1 regularized plan optimized with respect to the nominal scenario. For each patient, λ was chosen such that the regularized plan resulted in a 10% cost to plan quality relative to the unregularized plan.

Patient	Metric	Unregularized		Reweighted l_1	
		Median	Range	Median	Range
1	PTV: D2% (Gy)	72.73	4.84	73.36	4.42
	PTV: D98% (Gy)	64.06	12.69	62.96	13.60
	Mandible: Dmax (Gy)	69.58	4.55	70.91	1.80
	Left Parotid: Dmean (Gy)	25.70	9.42	17.76	8.14
2	PTV: D2% (Gy)	71.03	2.48	73.58	3.97
	PTV: D98% (Gy)	64.89	9.07	64.18	9.89
	Mandible: Dmax (Gy)	65.80	19.66	67.26	18.00
	Left Parotid: Dmean (Gy)	1.15	1.16	2.32	2.08
	Right Parotid: Dmean (Gy)	2.71	3.22	0.87	1.55
3	PTV: D2% (Gy)	71.66	4.08	72.73	5.33
	PTV: D98% (Gy)	64.30	11.23	62.54	12.01
	Mandible: Dmax (Gy)	67.33	5.63	67.12	3.31
	Left Parotid: Dmean (Gy)	25.61	6.28	25.80	9.45
	Spinal Cord: Dmax (Gy)	26.79	35.76	23.50	34.56
4	PTV: D2% (Gy)	71.29	7.97	71.85	7.62
	PTV: D98% (Gy)	64.21	12.14	63.16	11.83
	Mandible: Dmax (Gy)	69.70	4.94	70.22	3.69
	Right Parotid: Dmean (Gy)	10.92	8.98	9.65	8.27
	Constrictors: Dmean (Gy)	4.58	5.70	4.55	5.72

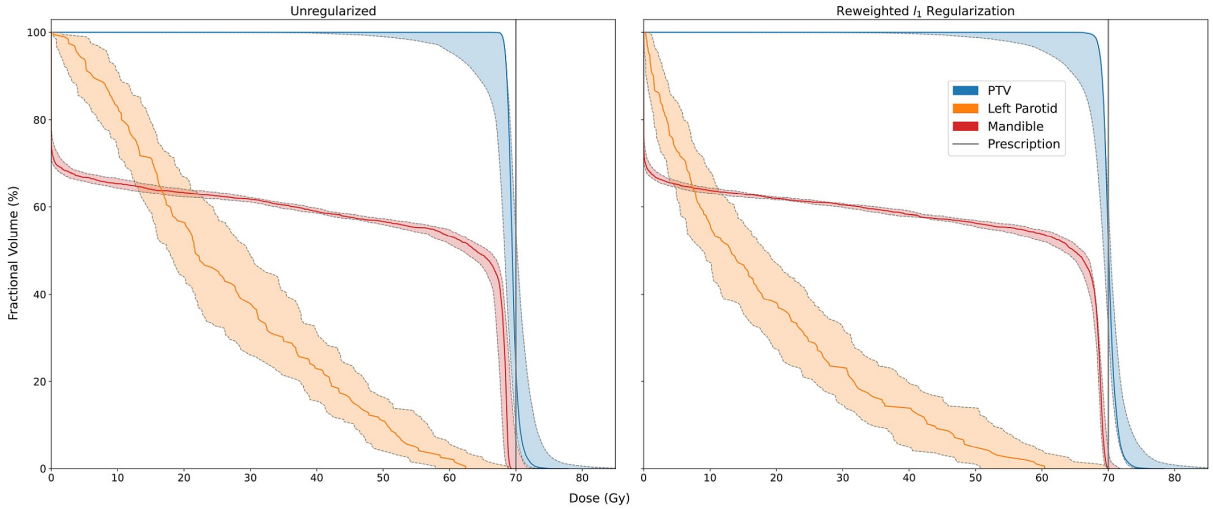

Figure S2: DVH bands across all uncertainty scenarios obtained from the unregularized plan and the reweighted l_1 regularized plan for patient 1. The solid lines indicate the DVH curves of the nominal scenario.

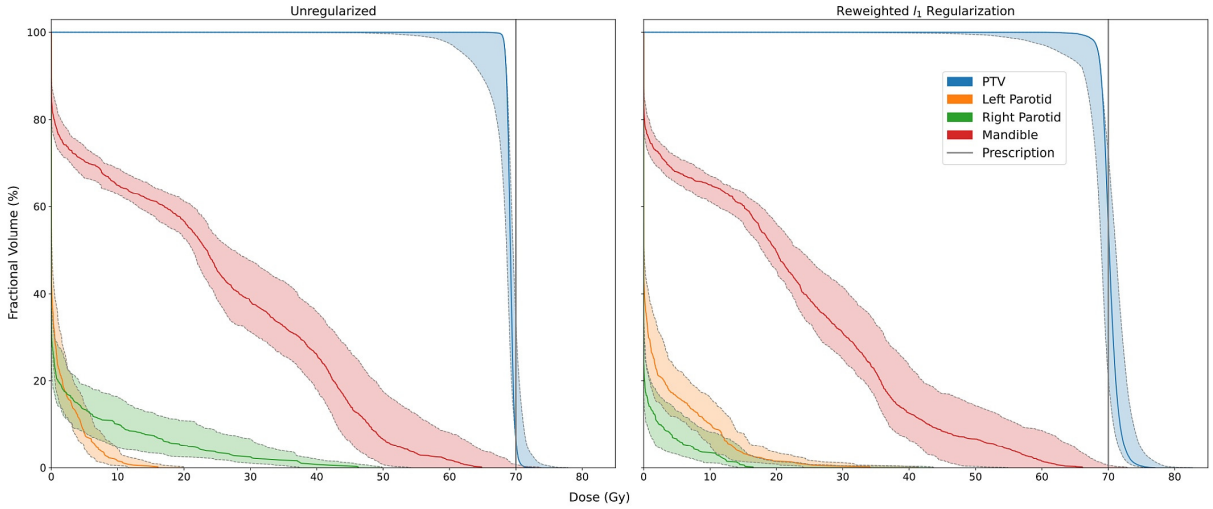

Figure S3: DVH bands across all uncertainty scenarios obtained from the unregularized plan and the reweighted l_1 regularized plan for patient 2. The solid lines indicate the DVH curves of the nominal scenario.

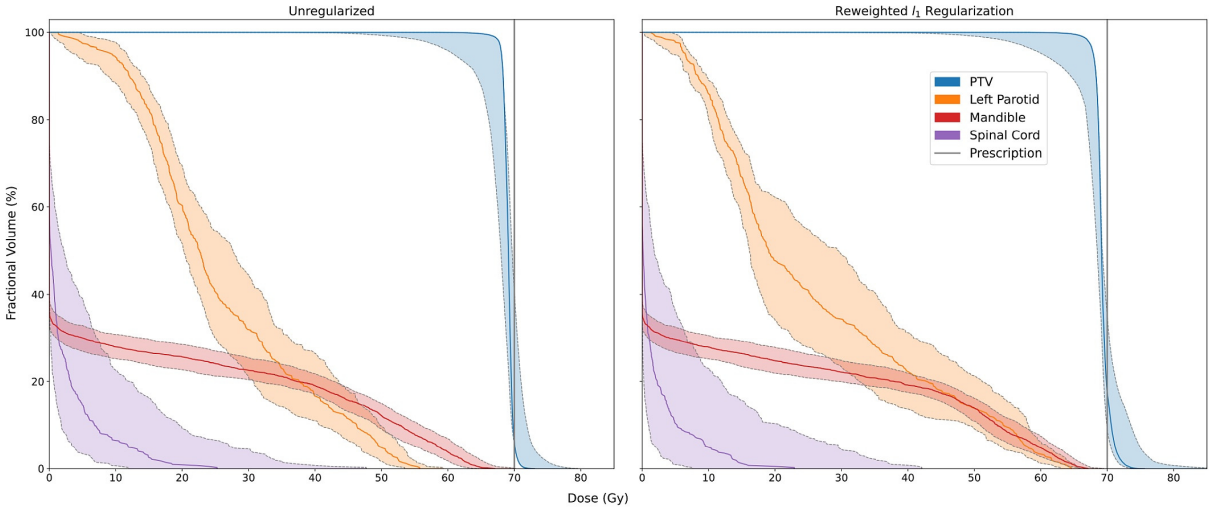

Figure S4: DVH bands across all uncertainty scenarios obtained from the unregularized plan and the reweighted l_1 regularized plan for patient 3. The solid lines indicate the DVH curves of the nominal scenario.

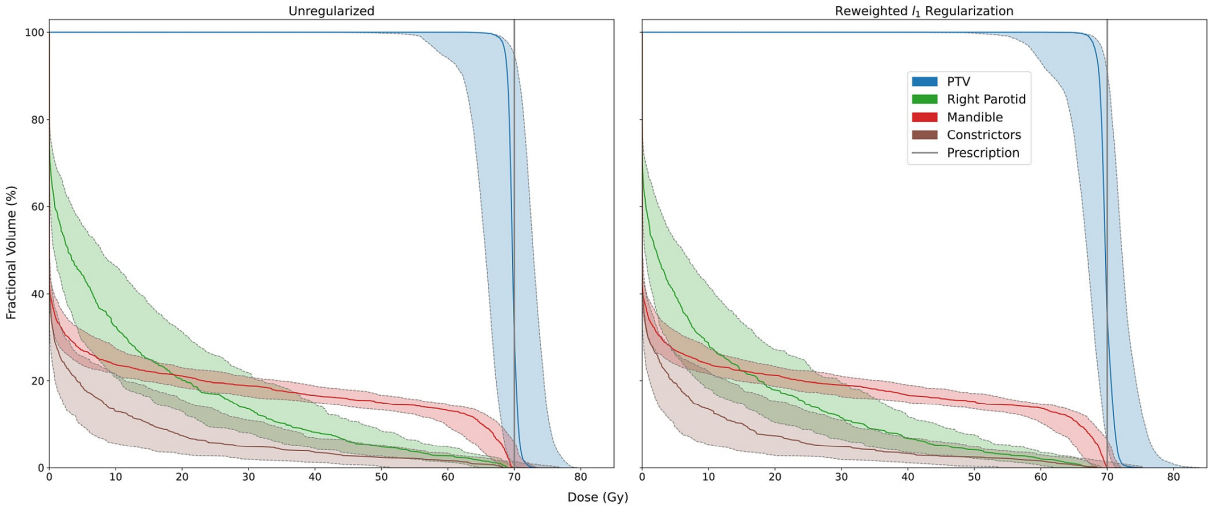

Figure S5: DVH bands across all uncertainty scenarios obtained from the unregularized plan and the reweighted l_1 regularized plan for patient 4. The solid lines indicate the DVH curves of the nominal scenario.